Nanoelectronics and Its New Materials – A NEW ERA OF NANOSCIENCE

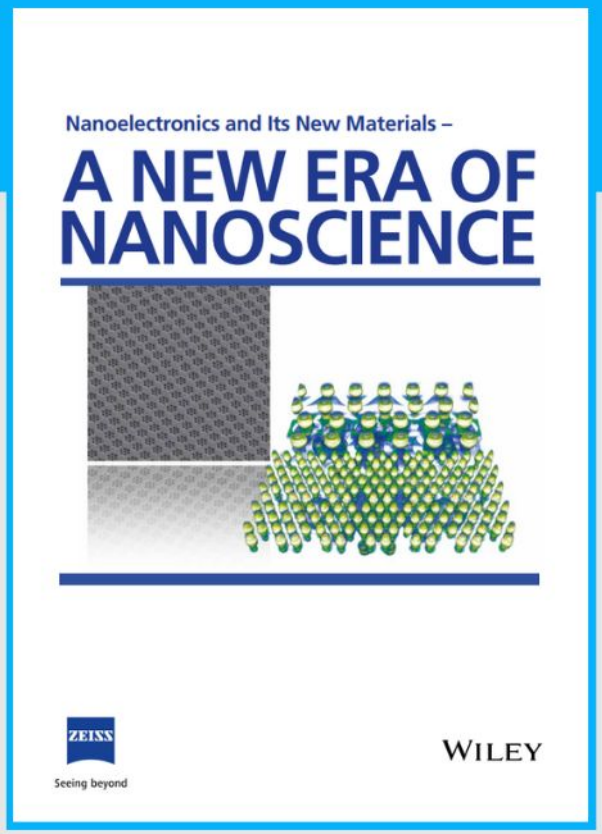

Discover the recent advances in electronics research and fundamental nanoscience.

Nanotechnology has become the driving force behind breakthroughs in engineering, materials science, physics, chemistry, and biological sciences. In this compendium, we delve into a wide range of novel applications that highlight recent advances in electronics research and fundamental nanoscience. From surface analysis and defect detection to tailored optical functionality and transparent nanowire electrodes, this eBook covers key topics that will revolutionize the future of electronics.

To get your hands on this valuable resource and unleash the power of nanotechnology, simply download the eBook now. Stay ahead of the curve and embrace the future of electronics with nanoscience as your guide.

ZEISS

Seeing beyond

WILEY

NANO · MICRO small
www.small-journal.com

Continuous Single-Crystalline GaN Film Grown on WS_2-Glass Wafer

Yue Yin, Bingyao Liu, Qi Chen, Zhaolong Chen, Fang Ren, Shuo Zhang, Zhetong Liu, Rong Wang, Meng Liang, Jianchang Yan, Jingyu Sun, Xiaoyan Yi, Tongbo Wei, Junxi Wang, Jinmin Li, Zhongfan Liu,* Peng Gao,* and Zhiqiang Liu**

Use of 2D materials as buffer layers has prospects in nitride epitaxy on symmetry mismatched substrates. However, the control of lattice arrangement via 2D materials at the heterointerface presents certain challenges. In this study, the epitaxy of single-crystalline GaN film on WS_2-glass wafer is successfully performed by using the strong polarity of WS_2 buffer layer and its perfectly matching lattice geometry with GaN. Furthermore, this study reveals that the first interfacial nitrogen layer plays a crucial role in the well-constructed interface by sharing electrons with both Ga and S atoms, enabling the single-crystalline stress-free GaN, as well as a violet light-emitting diode. This study paves a way for the heterogeneous integration of semiconductors and creates opportunities to break through the design and performance limitations, which are induced by substrate restriction, of the devices.

1. Introduction

To achieve a well-defined orientation of the epilayer, conventional epitaxy of semiconductor films requires substrates with an identical (homoepitaxy) or compatible atomic arrangement (heteroepitaxy).[1] Homoepitaxy generally produces satisfactory crystal quality,[2] while in heteroepitaxy, lattice constant mismatch usually results in excessive accumulation of strain and deterioration of material quality. Fortunately, strain engineering could promote lattice mismatch tolerance to some extent.[3] However, symmetry matching at the interface remains rigid, thus, significantly limiting the manipulation, integration, and utilization of different functional films by means of epitaxy.[4] Therefore, symmetry mismatched epitaxy is highly desired.

Recently, the growth of high-quality semiconductors (nitrides, arsenides) on highly lattice-mismatched substrates has been demonstrated via 2D materials assisted remote epitaxy mode.[5] In this case, the strength of interfacial interactions can be controlled by the thickness and polarity of the 2D material. Especially, the orientation of the epilayer is still guided by the lattice of single crystalline substrates.[6]

However, evidently, such remote epitaxy mode does not work due to the lack of lattice guide from the substrate, therefore, new strategy for growing single-crystalline nitride film on amorphous substrate is still under exploration. Choi et al. reported the fabrication of discrete nitride pyramid arrays on amorphous glass with the assistance of a titanium pre-orienting layer. However, their in-plane orientations were still random,[7] indicating that the metal preorienting layer strategy is not capable of nitride epitaxy relationship regulation.

Y. Yin, Q. Chen, F. Ren, S. Zhang, M. Liang, J. Yan, X. Yi, T. Wei, J. Wang, J. Li, Z. Liu
Research and Development Center for Semiconductor Lighting Technology
Institute of Semiconductors
Chinese Academy of Sciences
Beijing 100083, China
E-mail: tbwei@semi.ac.cn; lzq@semi.ac.cn

Y. Yin, Q. Chen, F. Ren, S. Zhang, M. Liang, J. Yan, X. Yi, T. Wei, J. Wang, J. Li, Z. Liu
Center of Materials Science and Optoelectronics Engineering
University of Chinese Academy of Sciences
Beijing 100049, China

B. Liu, Z. Liu, P. Gao
Electron Microscopy Laboratory
and International Center for Quantum Materials
School of Physics
Peking University
Beijing 100871, China
E-mail: p-gao@pku.edu.cn

The ORCID identification number(s) for the author(s) of this article can be found under https://doi.org/10.1002/smll.202202529.

B. Liu, Z. Liu, Z. Liu
Academy for Advanced Interdisciplinary Studies
Peking University
Beijing 100871, China
E-mail: zfliu@pku.edu.cn

B. Liu, Z. Chen, Z. Liu, R. Wang, J. Sun, Z. Liu
Beijing Graphene Institute (BGI)
Beijing 100095, China

Z. Chen, Z. Liu
Center for Nanochemistry (CNC)
Beijing Science and Engineering Center for Nanocarbons
Beijing National Laboratory for Molecular Sciences
College of Chemistry and Molecular Engineering
Peking University
Beijing 100871, China

J. Sun
College of Energy
Soochow Institute for Energy and Materials Innovations
Jiangsu Provincial Key Laboratory for Advanced Carbon Materials and Wearable Energy Technologies
Soochow University
Suzhou 215006, China

DOI: 10.1002/smll.202202529

2D material is another promising candidate to modulate the nitride epitaxy on the amorphous substrate. Graphene is used because of its mature synthesis technology and compatible structure with nitrides.[8] Unfortunately, due to the weak interaction and large lattice mismatch between graphene and nitride epilayer, it is difficult to control the lattice orientations of the epilayer, especially for the *ab* plane.[9] For the growing GaN on quartz glass, our group proposed the nanorod-assisted van der Waals epitaxy strategy, which included narrowing down the in-plane orientations of the GaN epilayers to three.[10] However, the single crystalline nitride epitaxy on the amorphous substrate assisted with graphene is still not realized, and the feasibility of semiconductor heterogeneous integration by epitaxy remains unconfirmed. Hence, it is a matter of urgency to find new applicable 2D materials for buffer layers.[11]

WS_2 is a noteworthy potential candidate for buffer layers owing to its stronger polarity and suitable geometric structure.[11e,f,12] Except for the small lattice mismatch (≈1%) with GaN and AlN, the atom arrangement of WS_2 is also significantly similar to that of nitrides. S atoms share the same spatial arrangement as N atoms in nitrides, which should provide a suitable template and ensure the feasibility of single-crystalline nitrides epitaxy.[13] Gupta et al. demonstrated the growth of single-crystalline GaN island on mechanically exfoliated WS_2 flakes and Hossain et al. further showed that thermally sulfurized WS_2 is also a proper buffer layer for GaN growth.[11f,14] Yu et al. reported that, besides transfer, directly growing WS_2 on GaN is also a promising strategy to fabricate WS_2/GaN p-n junction.[15] Despite this remarkable progress in the WS_2 and GaN system, the epitaxial growth of single-crystalline GaN film on WS_2, which could expand the range of supporting substrates, that is, glass, in our case, and the interface of GaN/WS_2 still remains challenging. In this work, we use WS_2 as the buffer layer and successfully achieve the epitaxy of single-crystalline GaN films on amorphous quartz glass for the first time. The calculations and experimental results verify that the first interfacial nitrogen layer plays a crucial role in the well-defined heterogeneous interface by forming a weak interaction with the three S atoms in WS_2 and covalent bonds with metal atoms, simultaneously. Moreover, the weak interaction with the WS_2-glass wafer prompts the GaN epilayer to exhibit homoepitaxial-level stress-free and easy exfoliation characteristics. Furthermore, profited by this device-quality GaN epilayer, we fabricated a 411 nm full functional violet light-emitting diode (LED). Our proposed strategy may fulfill the epitaxy of large-area single-crystalline semiconductor materials on symmetrically mismatched substrates, which would provide opportunities for heterogeneous integration and matter assembly, that is, integrating semiconductors with different symmetries into a multifunctional system.

2. Results

Initially, we attempt to perform the epitaxy of GaN films on quartz glass with a graphene buffer layer. Predictably, grain boundaries and in-plane misorientations are found, as shown in Figure S1 (Supporting Information). Next, we investigate the surface morphology of the GaN epilayer by scanning electron microscopy (SEM) (Figure S1a, Supporting Information). Compared to the region without graphene (Figure S1b, Supporting Information), the GaN epilayer on graphene/quartz glass coalesces, however, numerous grain boundaries still exist. X-ray diffraction (XRD) azimuthal off-axis phi scan of GaN ($10\bar{1}3$) plane reveals (Figure S1c, Supporting Information) polycrystalline characteristic of the GaN epilayer. Furthermore, the electron backscatter diffraction (EBSD) inverse pole figure (IPF) colored orientation (X-, Y-, and Z-direction) mappings (Figure S1d–f, Supporting Information) confirm crystallographic orientation. The Z-direction EBSD mapping indicates that the as-grown GaN film has a single out-of-plane orientation, but the inconsistent colors in the X- and Y-directions demonstrate the disordered in-plane orientations of the as-grown GaN thin film, which is mainly attributed to the large lattice mismatch and weak interaction between the GaN and graphene. This is consistent with our previous work, where the film obtained from the graphene buffer layer is found to be a nearly single crystalline film and contains three preferred orientations with domain boundaries despite of using the state-of-the-art nanorod-assisted van der Waals epitaxy strategy, which enables to partly control the in-plane orientation of the GaN epilayer.[10]

WS_2 is regarded as a more promising candidate for GaN epitaxy on quartz glass owing to its polarity and lattice matching with GaN. First-principles energy and electronic structure calculations provide an opportunity to verify the rule of WS_2 as the buffer layer for nitrides epitaxy. The formation energy of N or Ga adatoms binding to three representative high symmetry sites of WS_2 (I hollow of the hexatomic ring, II top of S atom, III top of W atom, Figure S2, Supporting Information) is calculated separately (**Figure 1**a), revealing that the N atoms adsorbing at the surface of WS_2, especially on the top of W atoms at the hollow of the S sublattice, is energetically favorable. The charge density difference (CDD) distribution of the GaN/WS_2 heterointerface is conveyed in Figure 1b,c. S atoms are found to exhibit sp^3-like threefold symmetry slight charge accumulation. The interfacial binding energy (Figure 1d) of the GaN/WS_2 interface is calculated to be 86 meV $Å^{-2}$, which is 1.5–2.5 times larger than that of the GaN/graphene interface,[10] however, over a magnitude lower than that of bulk GaN.[16] Unlike graphene's case,[10] the interaction between WS_2 and GaN is considered to be strong enough to confine the lattice of the GaN epilayer. Single-crystalline GaN could be directly grown on WS_2 without the participation of the nanorod buffer layer. As a result, the epitaxial procedure of the GaN grown on amorphous substrates could be simplified. Bader analysis is further conducted to attain quantitative charge transfer between the WS_2 interlayer and the GaN epilayer by conducting on the valence charge using the complete charge as a reference.[17] The results show that the interfacial N atom donated only 0.075 e and the S atom donated 0.033 e per bond to perform a weak interaction.[18] It is consistent with the calculated binding energy of the GaN/WS_2 interface. Thus, it is reasonable to speculate that each N atom at the interface can still preserve 5.9 electrons and bind with three Ga or Al atoms to form covalent bonds similar to those in bulks. Based on the calculation results, epitaxy is performed to verify whether it is possible to grow single-crystalline GaN films on amorphous glass substrate using the WS_2 buffer layer. The crucial processes of growing GaN films on quartz glass

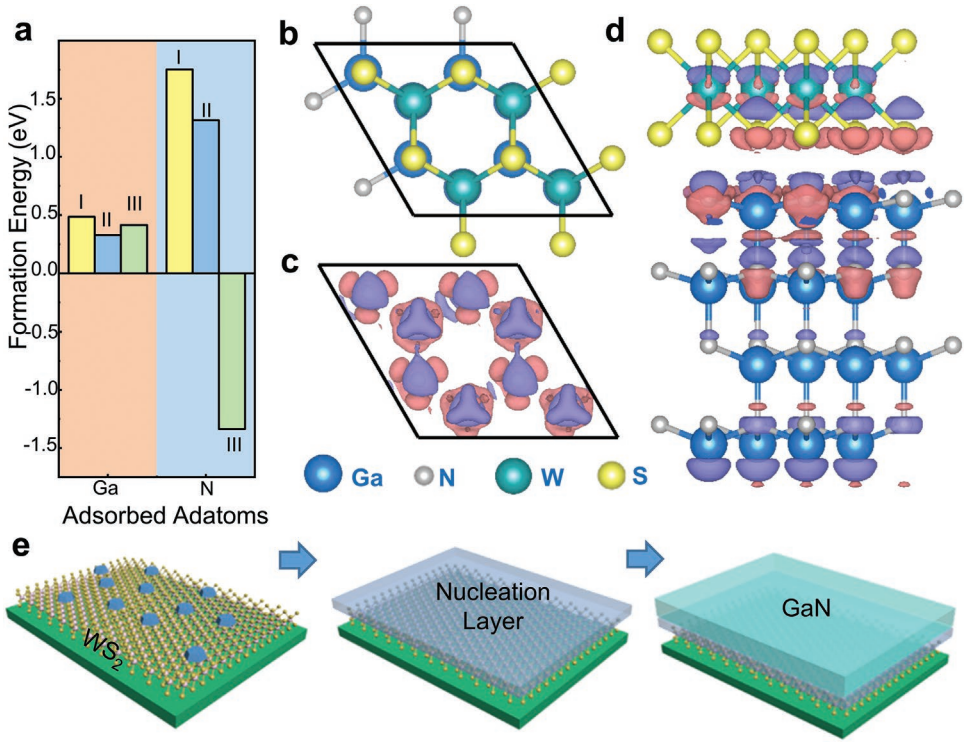

Figure 1. Electronic structure and schematic diagram of the nitrides epitaxy on WS_2. a) The formation energy of three representative structures with N or Ga procedures. Plan-view of b) atomic configuration of the epitaxial heterointerface and c) CDD isosurface map. d) Atomic model structures and CDD isosurfaces at the periphery of the $Al_xGa_{1-x}N/WS_2$ heterointerface. e) Schematic diagram of the key steps involved in the growth of GaN films on WS_2-glass wafer.

using the transferred WS_2 as the interlayer are schematically shown in Figure 1e.

We successfully transfer 1 cm^2 WS_2 onto a glass substrate with good uniformity, which is confirmed by the similar intensity of the 2LA and A_{1g} peaks in the Raman spectra (Figure S3e, Supporting Information).[19] However, due to the wet transfer process, some inevitable wrinkles appear (Figure S3c, Supporting Information), inducing a rougher surface topology (Figure S3b,d, Supporting Information).

Based on our calculation results, NH_3 is first introduced for WS_2 nitridation. Then, to promote the uniformity of the nucleation, a low-temperature (LT, 650 °C) $Al_xGa_{1-x}N$ nucleation layer is used considering the high adsorption energy and low migration barrier of Al atoms on WS_2 and decomposition problem at high temperature of WS_2.[5b,20]

Interruption growth is adopted to analyze the evolution of WS_2 at the interface. After nucleation, the interface is exploited by Raman spectra (**Figure 2**a) at five representative positions (Figure 2b), thus verifying the existence of a continuous WS_2 buffer layer. Moreover, a scanning transmission electron microscopy-high angle annular dark-field (STEM-HAADF) image of the interface clearly reveals the good lattice of the WS_2 layer and the well-aligned growth direction of $Al_xGa_{1-x}N$ (Figure 2c). Furthermore, energy dispersive X-ray spectroscopy (EDS) mappings of the involved elements and corresponding HAADF image (Figure 2d) also demonstrate the sandwich structure of the WS_2 buffer layer between the nitride epilayer and the quartz glass substrate after the LT nucleation procedure. Subsequently, the high-temperature (HT) GaN epitaxy process is carried out. We find that the 2LA mode peak of WS_2 in the Raman spectrum decreases and even vanishes (Figure S4a, Supporting Information), which can be attributed to the high-density structural defects induced during the long-time HT growth with NH_3, for example, S vacancies.[21] However, the high-resolution transmission electron microscopy (HRTEM) image in Figure 2e provides evidence that a WS_2 layer is still embedded under the $Al_xGa_{1-x}N$ template after HT growth, although its quality degrades, as confirmed by the EDS mappings across the interface (Figure 2f). Furthermore, the HADDF image shows a good lattice structure of the n-GaN epilayer in Figure S4b (Supporting Information), which demonstrates single-crystalline GaN without any observable defects or domain boundaries in the field of view. The integrated differential phase contrast (iDPC) image near the interface (Figure 2g) reveals that the GaN atomic columns have an ABAB stacking order and Ga polarity, which fits well with our calculated interface structure. These results indicate that introducing an LT-$Al_xGa_{1-x}N$ nucleation layer could be a reliable method for growing a single-crystalline GaN epilayer on the WS_2-glass wafer. Because the growth temperature for the $Al_xGa_{1-x}N$ nucleation layer is lower than that for the decomposition temperature of WS_2, the lattice of the LT-$Al_xGa_{1-x}N$ nucleation layer could be well guided by the interaction at the nitrides/WS_2 interface, and thus the obtained LT-$Al_xGa_{1-x}N$ can serve as a good template for the subsequent HT-GaN growth. During the HT-GaN epitaxy process, although WS_2 becomes defective to some extent, the crystalline

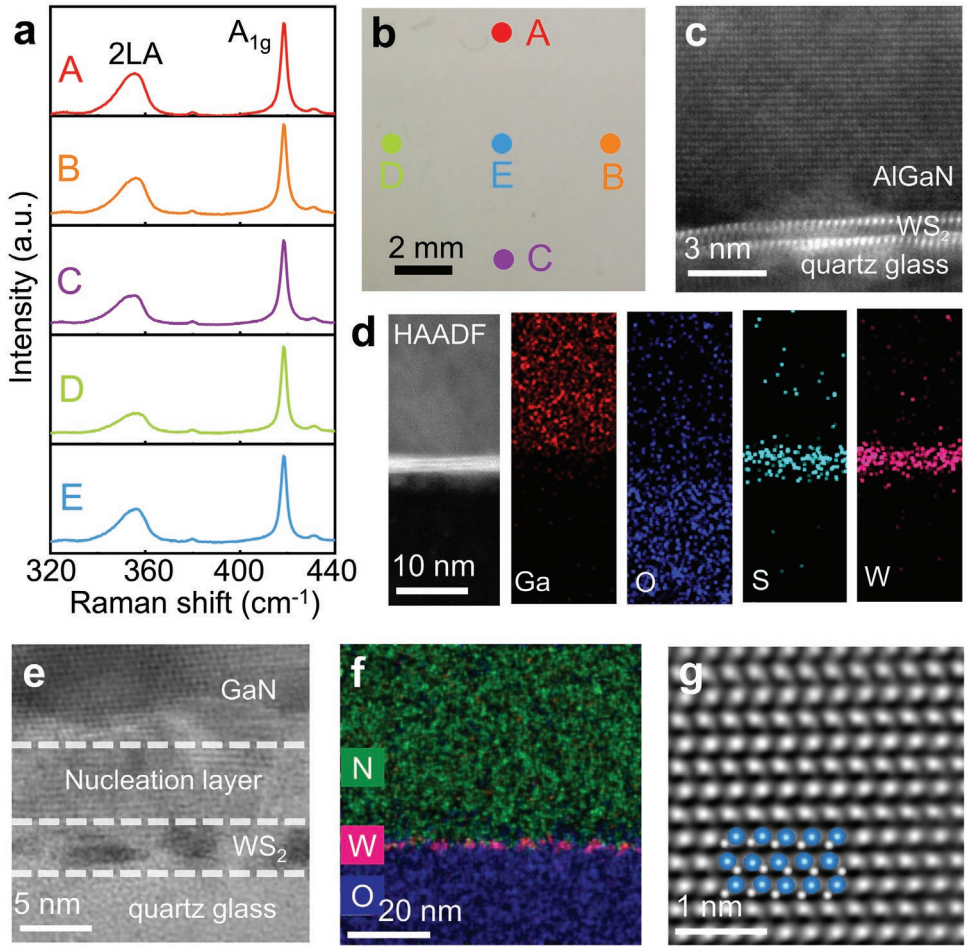

Figure 2. Evolution from $Al_xGa_{1-x}N$ nucleation to single-crystal film. a) Representative Raman spectra of the WS_2 films after the LT $Al_xGa_{1-x}N$ nucleation. b) Schematic of measured points on the WS_2-glass wafer. c) HAADF image of the $Al_xGa_{1-x}N/WS_2$/quartz glass interface after nucleation. d) HAADF image of the $Al_xGa_{1-x}N/WS_2$/quartz glass interface after nucleation and corresponding EDS mapping of Ga (red), O (blue), S (cyan), and W (pink) elements. e,f) HRTEM and EDS mapping image of the $Al_xGa_{1-x}N/WS_2$/quartz glass interface after the film epitaxy. g) iDPC image of GaN near the interface revealing that the epitaxial layer is Ga-polarity.

of the $Al_xGa_{1-x}N$ layer is retained and could sufficiently guide the lattice of the GaN epilayer.

The surface morphology of the as-grown film is investigated through plan-view SEM, as shown in **Figure 3**a, demonstrating that the GaN epilayer has completely coalesced. Compared to the GaN epilayer grown on the graphene buffer layer (Figure S1a, Supporting Information), the GaN epilayer grown on the WS_2 buffer layer exhibits a much flatter surface and fewer boundaries. The morphology of the GaN epilayer is further evaluated by atomic force microscope (AFM), showing a root mean square (RMS) roughness of ≈1.898 nm in a scanned area of 2×2 μm^2 (Figure 3b). Owing to the weak interaction at the heterointerface, the as-grown GaN epilayer is almost stress-free[22] (Figure 3c) and could be exfoliated easily (Figure 3f), which may benefit the growth of high-quality,[20b] high-In doping,[8c] and nitride alloying,[23] as well as the fabrication of flexible devices.

The crystallinity of the as-grown GaN epilayer on WS_2-glass wafer is later characterized by X-ray diffraction. In the 2θ scan shown in Figure 3d, only two diffraction peaks at 34.56° and 72.92° corresponding to the (0002) and (0004) planes of GaN, respectively, are observed, indicating its wurtzite structure with an aligned *c*-axis.[8a] The full width at half maximum (FWHM) of the GaN (0002) rocking curve is 1.6° (Figure 3d), and the screw dislocation density is estimated to be 6.67×10^{10} cm^{-2}. Meanwhile, the azimuthal off-axis phi scan of GaN ($10\bar{1}3$) reflection is performed (Figure 3e). Only one set of 60° periodic peaks shows that the GaN epilayer has a hexagonal structure and a uniform in-plane orientation, which is consistent with the EBSD mapping results (Figure 3g–i). These results highlight the remarkable orientation guidance of the WS_2 buffer layer for the growth of a single-crystalline GaN film, although the quality of the film is still limited by the quality of the underlying WS_2 layer.

Such a single-crystalline GaN epilayer obtained on WS_2-glass wafer enables visible LED fabrication. Its structure, which is composed of five-period multiquantum wells (MQWs) sandwiched between n-GaN and p-GaN layers, is illustrated in **Figure 4**a. The X-ray ω-scan reveals fourth satellite peaks of the $In_xGa_{1-x}N$/GaN MQWs (Figure 4b), indicating the uniform

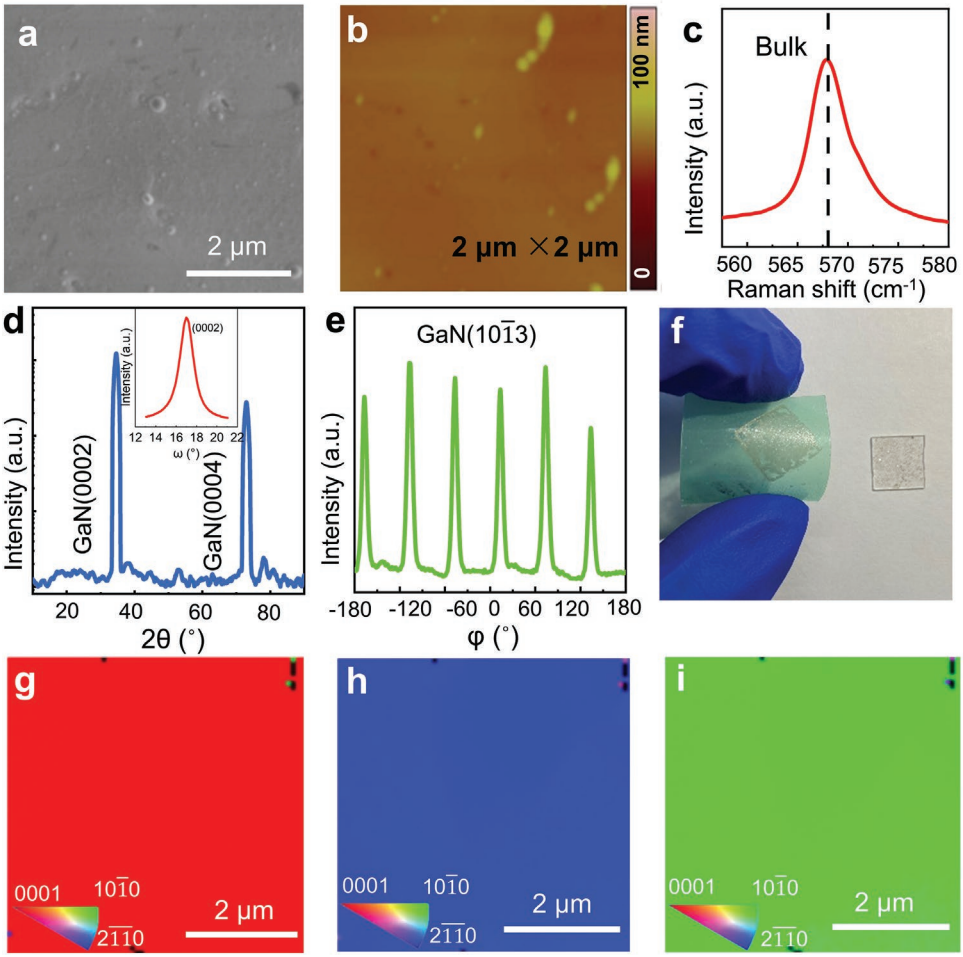

Figure 3. Characterizations of the single-crystal GaN film grown on the WS_2-glass wafer. a) SEM image of the obtained continuous GaN films on WS_2-glass wafer. b) AFM image of the as-grown GaN films with RMS roughness of ≈1.898 nm. c) Raman spectra of the as-grown GaN film on the WS_2-glass wafer. d) XRD-2θ spectrum of GaN, the inset is the XRD rocking curve of GaN (0002). e) XRD-φ scan of GaN (10$\bar{1}$3) direction. Probed area: 1 × 10 mm^2. f) GaN epilayer after exfoliating. g–i) Z-, X- and Y-direction EBSD IPF images of GaN film grown on WS_2-glass wafer.

thickness of $In_xGa_{1-x}N$ and sharp interfaces,[24] which is also confirmed by the HAADF image (Figure 4e). The EDS mapping and line profile of In element confirm its relative uniform distribution (Figure 4f,g). The interplanar spacing of $In_xGa_{1-x}N$ and GaN is measured to be 5.35 and 5.26 Å (Figure 4h), respectively, corresponding to the *d*-spacing of the hexagonal phase (wurtzite structure) GaN (0001) plane.[20b] We further investigate the optical property of the LED obtained on the WS_2-glass wafer through PL spectroscopy. The photograph (Figure S5a, Supporting Information) shows a violet emission at room temperature, consistent with the main peak of the room-temperature PL spectrum (Figure 4c) at 411 nm. Furthermore, we measure the temperature-dependent PL spectra (Figure 4d) from 8 to 300 K. Assuming the internal quantum efficiency (IQE) at 8 K is 100%, the IQE of this visible LED is calculated to be 16.8%.[25] Besides, from 8 to 300 K, we notice the unusual existence of a long-wavelength shoulder. In addition, in the early stage of nitride $In_xGa_{1-x}N$/GaN MQW LEDs, a similar long-wavelength shoulder is found which becomes more pronounced with the increasing In composition.[26] Considering the crystal quality of our sample, this shoulder should relate to the dislocation and their often-associated V-defect, which often result in inhomogeneous In distribution.[27] The suppression of such shoulder peak can be achieved by further growth optimization. The electroluminescence (EL) emission is shown in Figure S5b (Supporting Information), showing a wavelength light-emitting pattern similar to that of the PL results. These results verify that the GaN thin film grown on WS_2-glass wafer is at the device-quality level.

3. Conclusion

In summary, we demonstrate an extreme case to manifest the feasibility of nitride epitaxy on an amorphous substrate via an atomic WS_2 buffer layer. It is found that the first layer of the nitrogen adatom simultaneously donates electrons to the S atoms performing weak interaction and to the top Ga atoms forming covalent bonds, which plays an important role in the interfacial lattice arrangement. Thereby, successfully performing epitaxy of a single-crystalline GaN film on WS_2-glass wafer. Our approach offers a method to achieve semiconductor

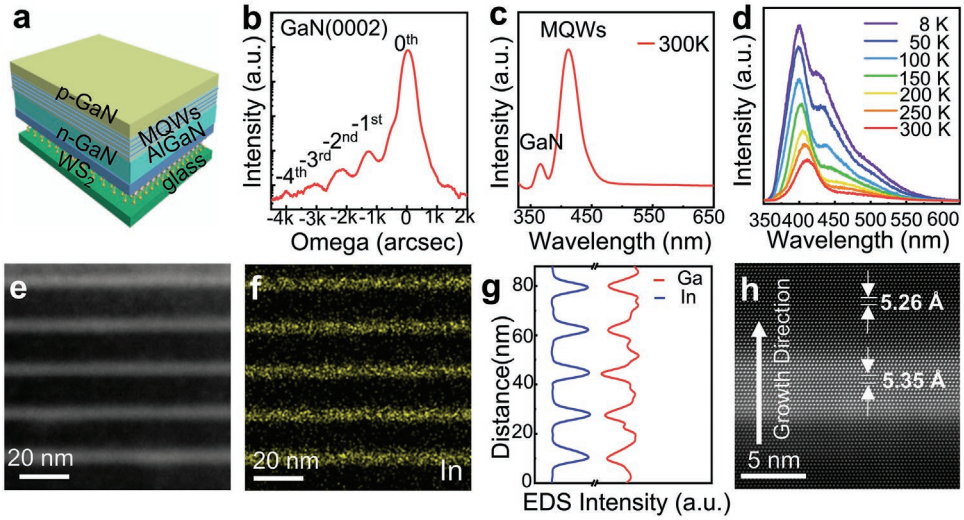

Figure 4. Structure and photoluminescence of as-fabricated LEDs on WS_2-glass wafer. a) Schematic of the LED structure. b) X-ray ω-scan of $In_xGa_{1-x}N$/GaN MQW lattice. c) Room-temperature PL spectrum of LEDs. d) Temperature-dependent PL spectra of LED. e) HADDF image of MQWs showing five pairs of GaN barriers and $In_xGa_{1-x}N$ wells. f) EDS mapping of In element in the MQWs. g) EDS line profile along vertical direction in (e) and (f). h) Atomically resolved HADDF image of MQWs.

epitaxy without the constraint of the substrate lattice. This approach could also serve as a realistic roadmap for the heterogeneous integration of semiconductors by epitaxy.

4. Experimental Section

CVD Growth of WS_2 on Sapphire Substrate and Transfer Process to Quartz Glass: To synthesize a continuous single-crystalline WS_2 film on sapphire substrates over an area of 1×1 cm^2, high-purity WO_3 and S were separately heated to 1000 and 200 °C under 200 sccm Ar and 20 sccm H_2, respectively. The obtained WS_2 was polycrystalline and its domain size of which was hundreds square microns. Hereafter, polymethyl methacrylate (PMMA) was spin-coated on WS_2/sapphire substrates as the released layer. Sapphire was etched by 2 mol L^{-1} KOH solution to separate with the PMMA /WS_2. After etching, the PMMA/WS_2 film was rinsed in DI water to clean the residues and attached to the quartz glass substrate before PMMA was removed by Propanol.

MOCVD Growth of GaN and LED Structure on WS_2-Glass Wafer: Trimethylgallium (TMGa), trimethylaluminum (TMAl), and NH_3 were used as Ga, Al, and N precursors separately. First, the nucleation layer was grown at 650 °C and 300 Torr for 20 min with TMGa, TMAl and NH_3 flows of 46.5, 135, and 36 000 sccm, respectively. Then the MOCVD chamber pressure was adjusted from 300 to 100 Torr and the temperature was raised to 1290 °C for 80 min of GaN epitaxy with TMGa and NH_3 flows of 360 and 36 000 sccm, respectively. To fabricate the $In_xGa_{1-x}N$-based LED structures, five-period $In_xGa_{1-x}N$/GaN MQWs were further grown on the GaN/WS_2/quartz glass template using triethylgallium (TEGa) as the Ga precursor. A Mg-doped p-GaN contact layer was subsequently deposited. H_2 was used as the carrier gas during the whole growth process. Any additional substrate treatments or intermediate layers were not applied.

LED Fabrication: The LED devices of 13×5 mil^2 size were fabricated using the conventional mesa technology. To enhance the current spread through electron beam evaporation, an indium tin oxide (ITO) (2000 Å) layer was deposited on the p-GaN layer. The mesa (1.75 µm) was manufactured by photolithography and inductively coupled etching. Cr/Al/Ti/Au (20/2000/500/3000 Å) multilayer metal film was adopted as p- and n-type Ohmic contact electrodes through electron beam evaporation. Subsequently, the SiO_2 passivation layer was deposited to protect the chip through plasma-enhanced chemical vapor deposition. Finally, the wafer was sliced into chips.

Transfer of the Epilayer: The epitaxial layer was mechanically exfoliated from the substrate using thermal release tape.

Characterization: The samples were characterized with SEM (SEM, Tokyo, Japan; operating at 3 kV), AFM (D3100, Veeco, New York, NY), XRD (Bede D1, UK; operated at 40 kV, 35 mA), PL (Horiba, Kyoto, Japan; 325 nm He-Cd laser with a power of 100 mW and cooled by liquid helium), Raman spectroscopy (Horiba, LabRAM HR-800, Japan; 532 nm laser excitation), EBSD (Zeiss, Jena, Germany), TEM (FEI Tecnai F20, operating at 200 kV), double aberration-corrected TEM (FEI Titan Cubed Themis G2 300; operating at 300 kV) and equipped EDS detector.

First-Principles Calculations: The projector augmented wave pseudopotential and the generalized gradient approximation of Perdew-Burke-Ernzerhof (PBE) were adopted as the exchange-correlation functional. Furthermore, the cutoff energy was set as 350 eV and full structural optimization when atomic forces are more than 0.02 eV Å^{-1} was performed. The optB88 exchange functional was chosen to model the van der Waals interactions. The interface systems were molded using supercells containing one layer of WS_2 and four layers of GaN. To maintain the symmetry of the wurtzite structure, the top layer of GaN was fixed. The vacuum region was set as 10 Å. A subtraction of the WS_2/GaN interface from the original stable geometry of the upper epitaxial layer can be obtained for each atom to analyze the Bader charge.

Supporting Information

Supporting Information is available from the Wiley Online Library or from the author.

Acknowledgements

Y.Y., B.Y.L., Q.C., and Z.L.C. contributed equally to this work. This work was supported by the National Key Research and Development Program of China (Grant Nos. 2019YFA0708202 and 2021YFB3600401), the National Natural Science Foundation of China (61974140 and 11974023), and the Youth Supporting Program of Institute of Semiconductors.

Conflict of Interest

The authors declare no conflict of interest.

Data Availability Statement

The data that support the findings of this study are available from the corresponding author upon reasonable request.

Keywords

2D materials, amorphous substrates, GaN, single-crystalline

Received: April 23, 2022
Revised: July 7, 2022
Published online: August 20, 2022

[1] a) J.-W. Lee, S. Tan, T.-H. Han, R. Wang, L. Zhang, C. Park, M. Yoon, C. Choi, M. Xu, M. E. Liao, S.-J. Lee, S. Nuryyeva, C. Zhu, K. Huynh, M. S. Goorsky, Y. Huang, X. Pan, Y. Yang, *Nat. Commun.* **2020**, *11*, 5514; b) Z. Lin, A. Yin, J. Mao, Y. Xia, N. Kempf, Q. He, Y. Wang, C.-Y. Chen, Y. Zhang, V. Ozolins, Z. Ren, Y. Huang, X. Duan, *Sci. Adv.* **2016**, *2*, e1600993.

[2] C. Kirchner, V. Schwegler, F. Eberhard, M. Kamp, K. J. Ebeling, K. Kornitzer, T. Ebner, K. Thonke, R. Sauer, P. Prystawko, M. Leszczynski, I. Grzegory, S. Porowski, *Appl. Phys. Lett.* **1999**, *75*, 1098.

[3] a) D. G. Schlom, L.-Q. Chen, C.-B. Eom, K. M. Rabe, S. K. Streiffer, J.-M. Triscone, *Annu. Rev. Mater. Res.* **2007**, *37*, 589; b) T. Z. Ward, J. D. Budai, Z. Gai, J. Z. Tischler, L. Yin, J. Shen, *Nat. Phys.* **2009**, *5*, 885.

[4] a) P. Krogstrup, N. L. B. Ziino, W. Chang, S. M. Albrecht, M. H. Madsen, E. Johnson, J. Nygård, C. M. Marcus, T. S. Jespersen, *Nat. Mater.* **2015**, *14*, 400; b) R. Yan, G. Khalsa, S. Vishwanath, Y. Han, J. Wright, S. Rouvimov, D. S. Katzer, N. Nepal, B. P. Downey, D. A. Muller, H. G. Xing, D. J. Meyer, D. Jena, *Nature* **2018**, *555*, 183.

[5] a) D. D. Liang, T. B. Wei, J. X. Wang, J. M. Li, *Nano Energy* **2020**, *69*, 104463; b) Y. Alaskar, S. Arafin, D. Wickramaratne, M. A. Zurbuchen, L. He, J. McKay, Q. Lin, M. S. Goorsky, R. K. Lake, K. L. Wang, *Adv. Funct. Mater.* **2014**, *24*, 6629; c) B. Liu, Q. Chen, Z. Chen, S. Yang, J. Shan, Z. Liu, Y. Yin, F. Ren, S. Zhang, R. Wang, M. Wu, R. Hou, T. Wei, J. Wang, J. Sun, J. Li, Z. Liu, Z. Liu, P. Gao, *Nano Lett.* **2022**, *22*, 3364.

[6] Y. Kim, S. S. Cruz, K. Lee, B. O. Alawode, C. Choi, Y. Song, J. M. Johnson, C. Heidelberger, W. Kong, S. Choi, K. Qiao, I. Almansouri, E. A. Fitzgerald, J. Kong, A. M. Kolpak, J. Hwang, J. Kim, *Nature* **2017**, *544*, 340.

[7] J. H. Choi, A. Zoulkarneev, S. I. Kim, C. W. Baik, M. H. Yang, S. S. Park, H. Suh, U. J. Kim, H. Bin Son, J. S. Lee, M. Kim, J. M. Kim, K. Kim, *Nat. Photonics* **2011**, *5*, 763.

[8] a) Y. Y. Wang, D. Dheeraj, Z. Q. Liu, M. Liang, Y. Li, X. Y. Yi, J. X. Wang, J. M. Li, H. Weman, *Cryst. Growth Des.* **2019**, *19*, 5516; b) Z. L. Chen, H. L. Chang, T. Cheng, T. B. Wei, R. Y. Wang, S. N. Yang, Z. P. Dou, B. Y. Liu, S. S. Zhang, Y. D. Xie, Z. Q. Liu, Y. F. Zhang, J. N. Li, F. Ding, P. Gao, Z. F. Liu, *Adv. Funct. Mater.* **2020**, *30*, 2001483; c) T. Journot, V. Bouchiat, B. Gayral, J. Dijon, B. Hyot, *ACS Appl. Mater. Interfaces* **2018**, *10*, 18857; d) Y. J. Hong, W. H. Lee, Y. P. Wu, R. S. Ruoff, T. Fukui, *Nano Lett.* **2012**, *12*, 1431; e) J. H. Park, J. Y. Lee, M. D. Park, J. H. Min, J. S. Lee, X. Yang, S. Kang, S. J. Kim, W. L. Jeong, H. Amano, D. S. Lee, *Adv. Mater. Interfaces* **2019**, *6*, 1900821; f) N. Nateghi, M. Samik, D. Cardinal, R. M. Jacobberger, A. J. Way, M. de la Mata, R. Martel, P. Desjardins, J. Arbiol, M. S. Arnold, O. Moutanabbir, *ECS Meet. Abstr.* **2020**, MA2020-01, 835; g) H. Chang, Z. Chen, B. Liu, S. Yang, D. Liang, Z. Dou, Y. Zhang, J. Yan, Z. Liu, Z. Zhang, J. Wang, J. Li, Z. Liu, P. Gao, T. Wei, *Adv. Sci.* **2020**, *7*, 2001272.

[9] W. Kong, H. S. Li, K. Qiao, Y. Kim, K. Lee, Y. F. Nie, D. Lee, T. Osadchy, R. J. Molnar, D. K. Gaskill, R. L. Myers-Ward, K. M. Daniels, Y. W. Zhang, S. Sundram, Y. Yu, S. H. Bae, S. Rajan, Y. Shao-Horn, K. Cho, A. Ougazzaden, J. C. Grossman, J. Kim, *Nat. Mater.* **2018**, *17*, 999.

[10] F. Ren, B. Liu, Z. Chen, Y. Yin, J. Sun, S. Zhang, B. Jiang, B. Liu, Z. Liu, J. Wang, M. Liang, G. Yuan, J. Yan, T. Wei, X. Yi, J. Wang, Y. Zhang, J. Li, P. Gao, Z. Liu, Z. Liu, *Sci. Adv.* **2021**, *7*, eabf5011.

[11] a) K. Chung, H. Oh, J. Jo, K. Lee, M. Kim, G. C. Yi, *NPG Asia Mater* **2017**, *9*, e410; b) M. Chubarov, T. H. Choudhury, D. R. Hickey, S. Bachu, T. Y. Zhang, A. Sebastian, A. Bansal, H. Y. Zhu, N. Trainor, S. Das, M. Terrones, N. Alem, J. M. Redwing, *ACS Nano* **2021**, *15*, 2532; c) Y. Kobayashi, K. Kumakura, T. Akasaka, T. Makimoto, *Nature* **2012**, *484*, 223; d) S. Karrakchou, S. Sundaram, T. Ayari, A. Mballo, P. Vuong, A. Srivastava, R. Gujrati, A. Ahaitouf, G. Patriarche, T. Leichle, S. Gautier, T. Moudakir, P. L. Voss, J. P. Salvestrini, A. Ougazzaden, *Sci. Rep.* **2020**, *10*, 21709; e) C. Zhao, T. K. Ng, C. C. Tseng, J. Li, Y. M. Shi, N. N. Wei, D. L. Zhang, G. B. Consiglio, A. Prabaswara, A. A. Alhamoud, A. M. Albadri, A. Y. Alyamani, X. X. Zhang, L. J. Li, B. S. Ooi, *RSC Adv.* **2017**, *7*, 26665; f) P. Gupta, A. A. Rahman, S. Subramanian, S. Gupta, A. Thamizhavel, T. Orlova, S. Rouvimov, S. Vishwanath, V. Protasenko, M. R. Laskar, H. G. Xing, D. Jena, A. Bhattacharya, *Sci. Rep.* **2016**, *6*, 23708.

[12] a) J. Lee, S. J. Yun, C. Seo, K. Cho, T. S. Kim, G. H. An, K. Kang, H. S. Lee, J. Kim, *Nano Lett.* **2021**, *21*, 43; b) C.-Y. Liu, H.-C. Huang, W. Choi, J. Kim, K. Jung, W. Sun, N. Tansu, W. Zhou, H.-C. Kuo, X. Li, *ACS Appl. Electron. Mater.* **2020**, *2*, 419.

[13] B. W. Zhou, X. H. Kong, S. Vanka, S. Chu, P. Ghamari, Y. C. Wang, N. Pant, I. S. Shih, H. Guo, Z. T. Mi, *Nat. Commun.* **2018**, *9*, 3856.

[14] E. Hossain, A. A. Rahman, A. P. Shah, B. A. Chalke, A. Bhattacharya, *Semicond. Sci. Technol.* **2020**, *35*, 035011.

[15] Y. Yu, P. W. Fong, S. Wang, C. Surya, *Sci. Rep.* **2016**, *6*, 37833.

[16] J. J. Wu, K. Wang, T. J. Yu, G. Y. Zhang, *Chin. Phys. B* **2015**, *24*, 068106.

[17] T. van Heerden, E. van Steen, *Faraday Discuss.* **2017**, *197*, 87.

[18] a) Y. Liu, E. S. Penev, B. I. Yakobson, *Angew. Chem., Int. Ed. Engl.* **2013**, *52*, 3156; b) Q. Ruan, L. Wang, K. V. Bets, B. I. Yakobson, *ACS Nano* **2021**, *15*, 18347.

[19] X. Zhang, X. F. Qiao, W. Shi, J. B. Wu, D. S. Jiang, P. H. Tan, *Chem. Soc. Rev.* **2015**, *44*, 2757.

[20] a) J. Y. Zhou, *Appl. Phys. Lett.* **2019**, *115*; b) Z. L. Chen, X. Zhang, Z. P. Dou, T. B. Wei, Z. Q. Liu, Y. Qi, H. N. Ci, Y. Y. Wang, Y. Li, H. L. Chang, J. C. Yan, S. Y. Yang, Y. F. Zhang, J. X. Wang, P. Gao, J. M. Li, Z. F. Liu, *Adv. Mater.* **2018**, *30*, 1801608.

[21] S. Mignuzzi, A. J. Pollard, N. Bonini, B. Brennan, I. S. Gilmore, M. A. Pimenta, D. Richards, D. Roy, *Phys. Rev. B* **2015**, *91*, 195411.

[22] a) Y. P. Wang, Y. Y. Sun, S. B. Zhang, T. M. Lu, J. Shi, *Appl. Phys. Lett.* **2016**, *108*, 013105; b) D. G. Zhao, S. J. Xu, M. H. Xie, S. Y. Tong, H. Yang, *Appl. Phys. Lett.* **2003**, *83*, 677.

[23] S. Zhang, X. R. Zhang, F. Ren, Y. Yin, T. Feng, W. R. Song, G. D. Wang, M. Liang, J. L. Xu, J. W. Wang, J. X. Wang, J. M. Li, X. Y. Yi, Z. Q. Liu, *J. Appl. Phys.* **2020**, *128*, 155705.

[24] T. Ayari, S. Sundaram, X. Li, Y. El Gmili, P. L. Voss, J. P. Salvestrini, A. Ougazzaden, *Appl. Phys. Lett.* **2016**, *108*, 171106.

[25] P. Henning, S. Sidikejiang, P. Horenburg, H. Bremers, U. Rossow, A. Hangleiter, *Appl. Phys. Lett.* **2021**, *119*, 011106.

[26] X. H. Wu, C. R. Elsass, A. Abare, M. Mack, S. Keller, P. M. Petroff, S. P. DenBaars, J. S. Speck, S. J. Rosner, *Appl. Phys. Lett.* **1998**, *72*, 692.

[27] M. A. Reshchikov, H. Morkoç, *J. Appl. Phys.* **2005**, *97*, 061301.